Preparation and characterization of fluoride-substituted apatites

L. J. JHA*‡, S. M. BEST‡, J. C. KNOWLES‡, I. REHMAN‡, J. D. SANTOS#, W. BONFIELD‡
*National Institute of Biomedical Engineering, #Department of Metallurgy, Faculty of Engineering, University of Porto, Rua dos Bragas, 4099 Porto, Portugal
‡Interdisciplinary Research Centre in Biomedical Materials, Queen Mary and Westfield College, University of London, Mile End Road, London E1 4NS, UK

Apatites were prepared with three different fluoride concentrations: 0.0 mM (pure hydroxyapatite) 2.5 mM and 5 mM. Reactions were performed in aqueous medium using a reaction between diammonium orthophosphate and calcium nitrate 4-hydrate and ammonium fluoride at temperatures of 3°, 25°, 60° and 90 °C. The effects of reaction temperature and fluoride concentration on the crystal morphology, phase purity and crystallinity of the precipitates were observed, using transmission electron microscopy (TEM), X-ray diffraction (XRD), Fourier transform infrared (FTIR) spectroscopy and ion chromatography. Transmission electron micrographs revealed that the crystallites precipitated at 3 °C were spheroidal, but became increasingly acicular with increasing precipitation temperature. X-ray diffraction results indicated that all the materials produced were phase pure and that the crystallinity of apatites prepared at higher precipitation temperatures was higher than those prepared at lower precipitation temperatures. A significant difference in the *a*-axis dimension of fluoride-substituted apatites was observed, as compared to hydroxyapatite. FTIR spectroscopy revealed a hydroxyl band at 3568 cm^{-1}, along with a broad peak of adsorbed water in the region of 3568 cm^{-1} to 2670 cm^{-1} in the hydroxyapatite and fluoride-substituted apatite powders. Hence by careful selection of the precipitation conditions and fluoride contents, the composition and morphology of fluoride-substituted apatite may be controlled and this has interesting implications for the development of these materials for biomedical implantation.

1. Introduction

Hard tissues in the human body are composites, consisting of a mixture of organic and inorganic phases. The mineral phase of bone comprises approximately 60 to 70% of the dry mass, while the remainder is composed of collagen and other organic compounds. Bone mineral is a calcium phosphate containing carbonate and small amounts of fluoride ions, sodium, magnesium, and other trace components [1].

The mineral phase of tooth enamel consists of apatite containing 0.04 wt % to 0.07 wt % of fluoride [2], and constitutes about 95 to 97% of the dry mass. Fluoride ions present in saliva and blood plasma, are required for normal dental and skeletal development. It has been suggested that a fluoride intake of 1.5–4 mg per day significantly reduces the risk of dental caries [3]. van den Hoek *et al.* [4] stated that the mechanisms by which dental caries are prevented by fluoride are not yet fully understood. However, it was suggested that prior to the eruption of teeth, fluoride is incorporated into the enamel in the form of fluorohydroxyapatite, which is more acid resistant than hydroxyapatite.

It has been reported in the literature [5–8] that the presence of fluoride ions in solutions containing calcium and phosphate ions promotes the formation of apatite minerals, usually by the enhancement of the rate of hydrolysis of phase intermediates. Moreno *et al.* [9] have suggested that fluoride has an effect on the magnitude of the driving force for precipitation, i.e. on the supersaturation of the solution with respect to the fluoride-containing phase which precipitates. Fluoride ion substitution for OH groups in the hydroxyapatite lattice has been found to be irreversible [4]. It is suggested that incorporation of fluoride ions into the apatite structure increases the crystallinity and the Ca/P ratio and decreases the HPO_4/PO_4 ratio. Several reviews [8, 10, 11] have reported the effects of fluoride concentrations on the formation of calcium fluoride (CaF_2), versus fluorapatite. It has been shown that the fluoride concentration required to convert hydroxyapatite (HA) to fluorapatite (FAp) increases with pH [12]. van den Hock *et al.* [4] suggested that FAp is deposited onto a growing surface in successive layers and that each layer of FAp forms only when the preceding

0957–4530

layer has attained equilibrium with the bulk solution.

It has been reported that apatite is the only calcium orthophosphate that can incorporate fluoride ions [4, 13]. However, dicalcium phosphate dihydrate has been described as readily taking up fluoride ions in the hydrolysis reactions to form FAp [13], suggesting that hydrolysis occurs more readily in fluoride solutions. Barone *et al.* [6] reported that fluoride ions promote the conversion of octacalcium phosphate to fluorapatite.

There have been some reports in the literature of the thermodynamic and kinetic effects of fluoride ion concentration on precipitation and dissolution reactions [5–8, 13–22]. However, the effects of preparation temperature on the crystal structure of precipitated fluoride-substituted apatite have not been comprehensively investigated.

In the present study, pure hydroxyapatite and fluoride-substituted apatites were prepared at 3, 25, 60 and 90 °C. The effects of fluoride ion substitution on the fluoride-substituted apatite structure were analysed using transmission electron microscopy (TEM), X-ray diffraction (XRD), Fourier transform infrared (FTIR) spectroscopy and ion chromatography.

2. Materials and methods

2.1. Precipitation method

AnalarR grade diammonium orthophosphate, calcium nitrate 4-hydrate and ammonium fluoride solutions were used to prepare pure hydroxyapatite and fluoride-substituted apatite at 3, 25, 60 and 90 °C. Ammonium fluoride was added in two different concentrations, 2.5 mM and 5 mM, to 1.8 litres of calcium nitrate solution heated at 60 °C. The solution was held at this temperature for 1 h and continuously stirred. Diammonium orthophosphate solution was added dropwise to constantly stirred calcium nitrate solution at a set temperature over a period of 2 h during precipitation. The precipitate was agitated at the set temperature for 1 h and then aged at 25 °C for 20 h. Samples were filtered using a Buchner funnel and washed five times using double-distilled water. The filter cakes were dried in an oven at 90 °C in a filtered air atmosphere for 20 h and then ground to powder.

The fluoride-substituted apatites prepared using 2.5 mM and 5 mM solutions of ammonium fluoride are referred to as HA025F and HA05F, respectively.

2.2. Transmission electron microscopy

The morphology of the precipitates was determined by transmission electron microscopy (JEOL JEM 100 CX). Carbon-coated 200 mesh copper grids were dipped in a dilute suspension of the precipitate. Excess suspension was carefully removed using absorbent paper, before being left to dry in air prior to insertion into the microscope. The precipitates were examined in bright field mode at a magnification of 50 000 × using an accelerating voltage of 100 kV. Selected area electron diffraction patterns were obtained for each of the precipitates. The camera length of the microscope was calibrated using a diffraction pattern from an evaporated aluminium standard sample.

2.3. Carbon, hydrogen and nitrogen analysis

Carbonate was determined as carbon using a Control Equipment Corporation Model 240 XA CH&N element analyser. The samples were dried at 120 °C for 24 h prior to analysis in order to remove adsorbed water. Duplicate measurements were taken for each sample.

2.4. Fluoride analysis

0.5 g of the sample was placed in 200 ml of double-distilled water. The suspension was distilled from sulphuric acid at 180 °C and the distillate collected in dilute sodium biocarbonate solution. The fluoride ion content was determined in the distillate using an ion chromatograph, Dionex DX 100.

2.5. X-ray diffraction

Following precipitation and drying of the powders, the samples were analysed using a Siemens D5000 diffractometer with a flat plate geometry. CuK_α radiation was used (wavelength 0.15418 nm) with a graphite diffracted beam monochromator. Data were collected from 5° to 110° 2θ, with a step size of 0.02° and a count time of 12 s.

2.5.1. Rietveld analysis

The crystal structures of HA and fluoride-substituted apatite were refined using the Rietveld method [23]. The starting model used in the refinement was based on a single crystal determination [24]. Peak shapes were modelled using a pseudo-Voigt distribution and an asymmetry parameter was refined. Scattering factors for neutral atoms were assumed. In each case, five background parameters, a scale factor, four peak shape parameters, cell parameters and a zero point correction were refined before variation of the structural parameters. Isotropic thermal parameters were refined for all atoms and a site occupancy parameter refined for the hydroxyl oxygen. The hydrogen atom was not located.

From the calculated data, a numerical index (dimensionless) of the overall distortion (D_{ind}) of the structure may be calculated from the PO_4 tetrahedra. The numerical index (D_{ind}) represents the deviation of the PO_4 tetrahedra from an optimal configuration and is derived from:

$$D_{ind} = \frac{\sum_{i=1}^{i=6}(\theta_i - 109.17)^2}{6} \qquad \text{(A)}$$

with θ = angle O–P–O.

2.6. FTIR spectroscopy

Fourier transform infrared (FTIR) spectroscopy was used to analyse the powder samples of hydroxyapatite and fluoride-substituted apatite. FTIR spectra were obtained using a Nicolet 800 spectrometer in conjunction with a MTech photo-acoustic (PAS) cell. A photo-acoustic signal was generated when infrared radiation absorbed by a sample was converted into heat within the sample. This heat diffused to the sample surface and into the adjacent atmosphere. Thermal expansion of the gas produced the PAS signal. The signal generation process isolated a layer extending beneath the sample's surface, which has a suitable optical density for analysis, without altering the sample. The technique directly measured the absorbance spectrum of this layer. Spectra were obtained at 4 cm^{-1} resolution, by averaging 128 scans. The sample chamber of the PAS cell was purged with helium gas and dried using magnesium perchlorate as a drying agent.

3. Results

Transmission electron micrographs of hydroxyapatite and fluoride-substituted apatite are shown in Figs 1–3. The hydroxyapatite crystals were smaller and more spheroidal at precipitation temperatures of 25 °C and below, and became increasingly large and more acicular as the precipitation temperature increased, as shown in Fig. 1. A similar trend was observed for HA025F and HA05F precipitates, as shown in Figs 2 and 3. Considering the effects of fluoride concentration on the morphology of the precipitated apatites, it was found that increasing fluoride ion concentration tended to reduce the aspect ratio of the crystallites produced. The electron diffraction patterns taken for the HA025F prepared at precipitation temperatures of 3 and 90 °C are shown in Fig. 3e and f, respectively. Fig. 3e demonstrates a more complete ring structure than Fig. 3f and this is due to the smaller crystals resulting from the 3 °C reaction. Similar results were obtained for HA and HA025F samples.

From ion chromatographic analysis, no fluoride ions were detected in the HA sample whereas concentrations of 0.18 wt % and 0.27 wt % were detected in the HA025F and HA05F samples respectively, when precipitated at 3 °C. CH&N analysis indicated that the CO_3^{2-} ions in the HA, HA025F and HA05F samples precipitated at 3 °C were constant at 1.0 wt %. X-ray diffraction spectra for HA025F and HA05F precipitated at 3 °C and 90°C are shown in Figs 4 and 5. It can be seen that the peaks are more clearly defined at 90 °C. Both spectra show that the materials contain no extraneous calcium phosphate phases. Unit cell dimensions (*a* and *c* axes) were calculated from Rietveld refinement. The results, summarized in Table I, indicate that for the 3 °C and the 90 °C reactions, there was a decrease in both the *a* and *c* axis dimensions with increasing fluoride ion concentration. Also, for each fluoride ion concentration, there was a decrease in *a* axis dimension and an increase in *c* axis dimension as the reaction temperature increased from 3 to 90 °C. A significant variation in the values of Ca(2)–OH bond length was observed for HA025F and HA05F at precipitation temperatures of 3 and 90 °C, as shown in Fig. 6. However, a very small variation in Ca(2)–OH bond length for the HA was found at precipitation temperatures of 3 and 90 °C. The variation in distortion index (%) of the prepared materials with respect to precipitation temperatures is shown in Fig. 7. In general, the distortion index of the materials produced at 90 °C was found to be lower than the distortion index of the materials produced at 3 °C.

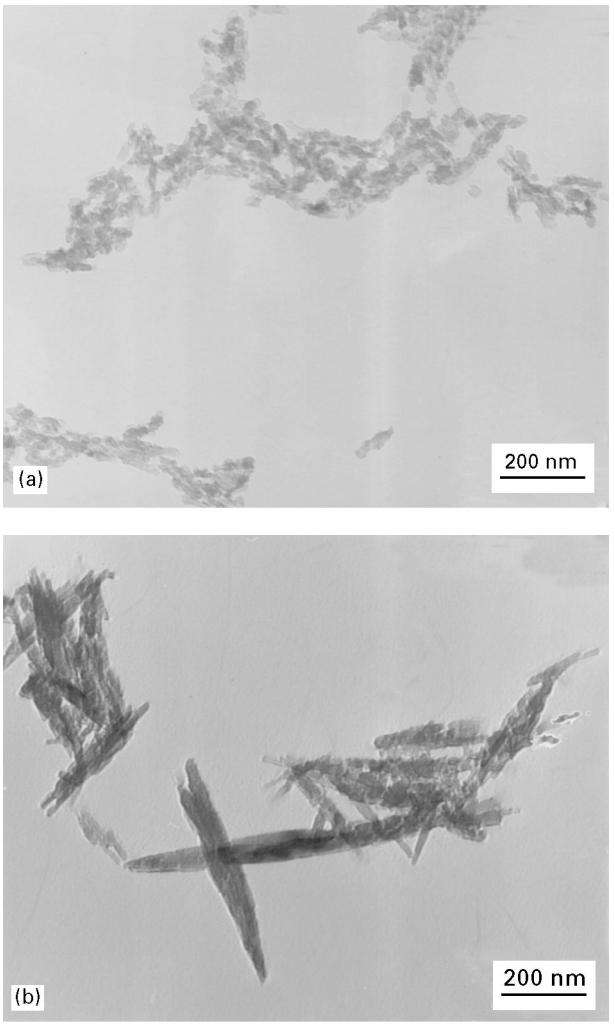

Figure 1 TEM micrographs of hydroxyapatite precipitated at (a) 25° C, (b) 60 °C.

PAS-FTIR spectra of the hydroxyapatite and fluoride-substituted apatite powders are shown in Figs 8 and 9. The spectra for HA, HA025F and HA05F revealed numerous peaks associated with phosphate bands at 600, 962 and 1025 cm^{-1}, carbonate bands at 875 cm^{-1}, 1418 cm^{-1} and 1455 cm^{-1} and a hydroxyl band at 3568 cm^{-1}, respectively. The hydroxyl band in the spectra of the HA025F and HA05F samples had a lower intensity than the HA sample. These spectra were also masked by a broad H_2O adsorption peak in the 2670 to 3568 cm^{-1} region.

4. Discussion

It was demonstrated that precipitation temperature has a strong influence on the morphology of precipitates of HA, HA025F and HA05F. This result may be

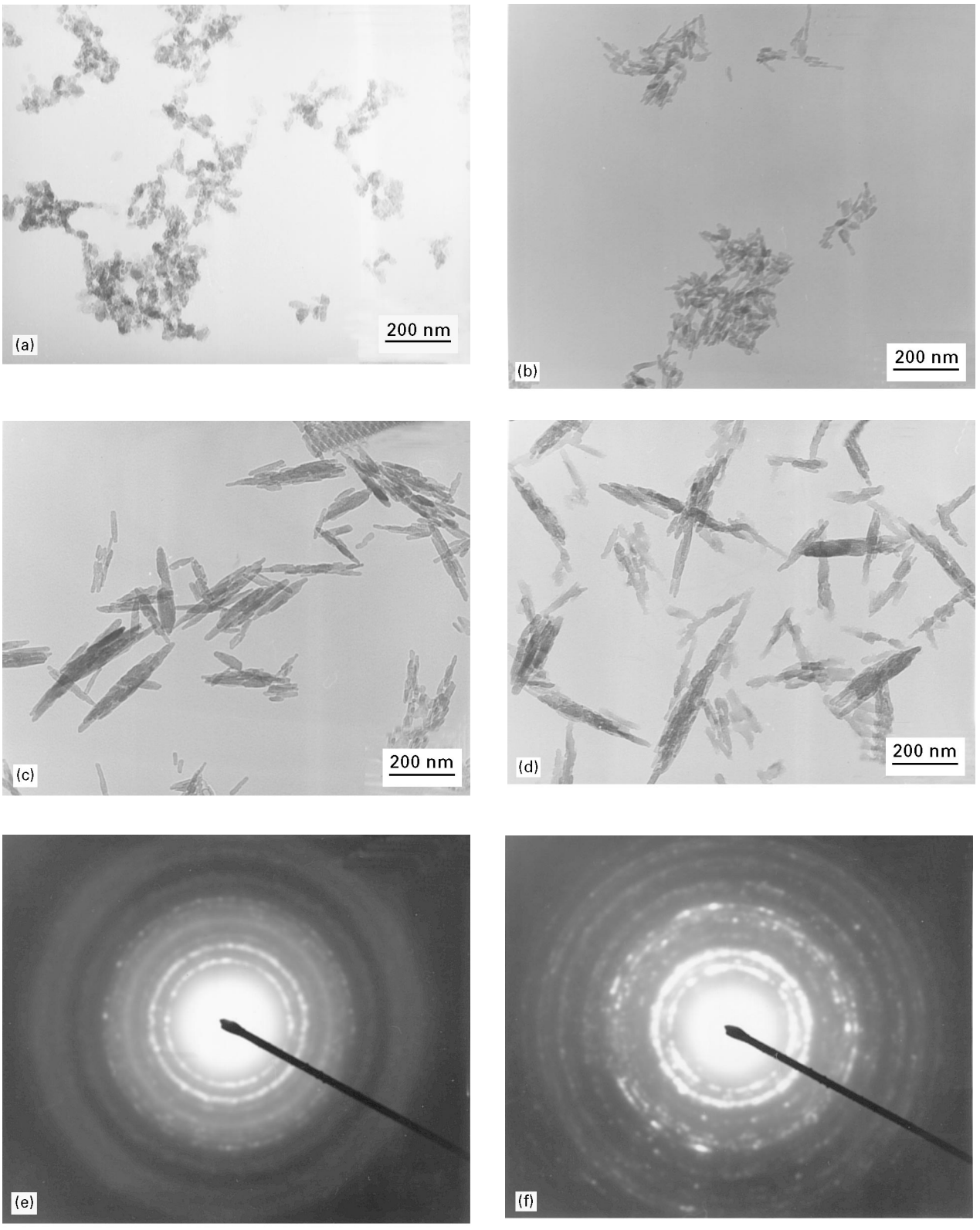

Figure 2 TEM micrographs of HA025F precipitated at (a) 3 °C, (b) 25 °C, (c) 60 °C and (d) 90 °C. Selected area electron diffraction patterns of HA025F precipitated at (e) 3 °C and (f) 90 °C.

explained on the basis that, as the precipitation temperature decreased from 90 °C to 3 °C, supersaturation of the solute increased. As a consequence, more apatite nucleation sites and a reduced apatite growth rate resulted in a much smaller precipitate size.

The peak height and peak area of the carbonate bands in HA, HA025F and HA05F powders were constant, irrespective of fluoride ion substitution. This observation for FTIR further supports the results obtained by CH&N analysis. The reduction in the OH peak height with increasing fluoride concentration suggests that the fluoride groups substituted for the OH groups. Therefore, it may be deduced that the changes which occurred in the lattices of HA025F and

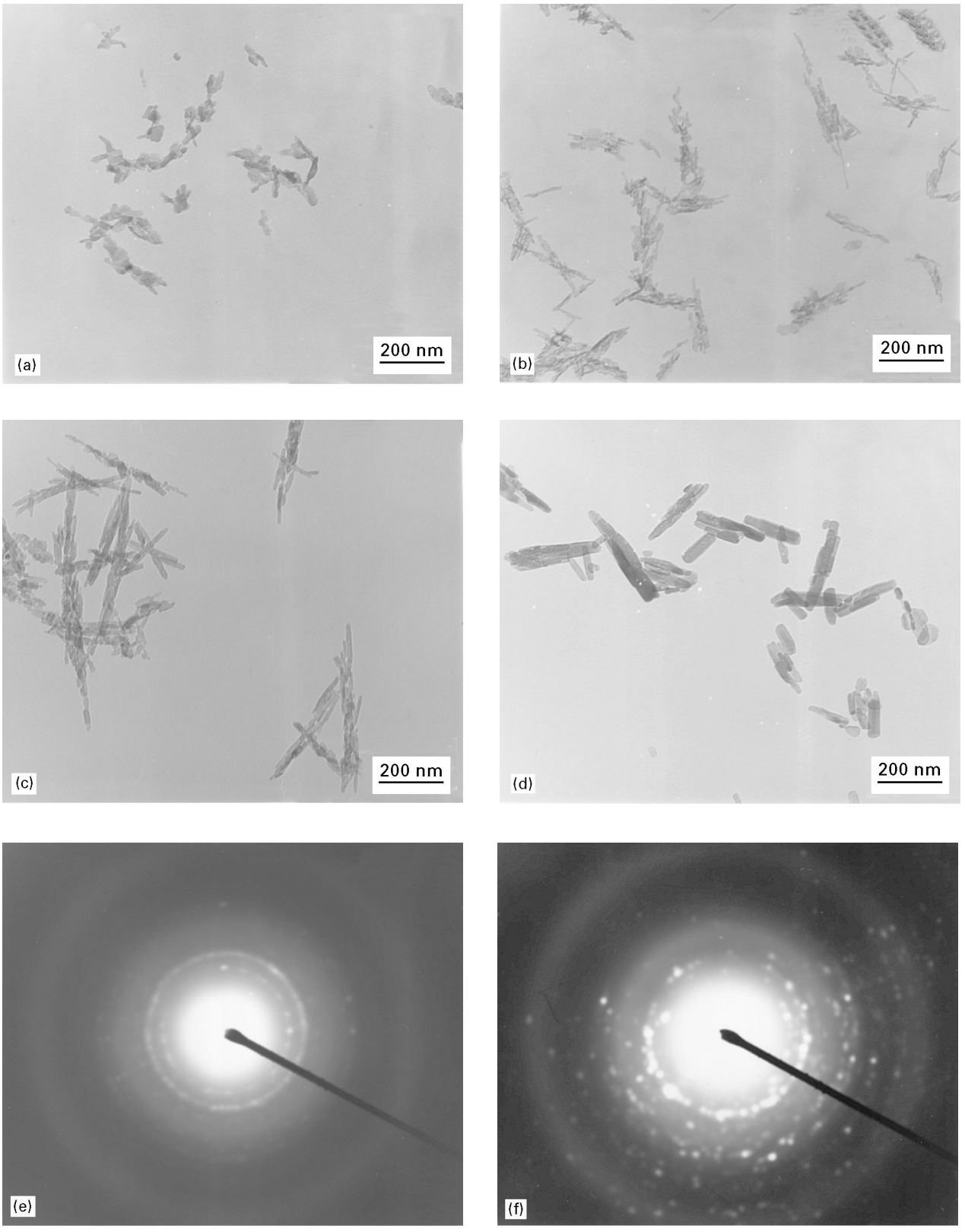

Figure 3 TEM micrographs of HA05F precipitated at (a) 3 °C, (b) 25 °C, (c) 60 °C and (d) 90 °C. Selected area electron diffraction patterns of HA05F precipitated at (e) 3 °C and (f) 90 °C.

HA05F compared with the HA were due to fluoride ion substitution for the hydroxyl group.

From the Rietveld refinement, it may be seen that there is a statistically significant difference in the *c*-axis length for samples precipitated at 90 °C as compared with the 3 °C samples. A more obvious decrease in the *a* axis dimension was observed in the fluoride-substituted apatites than in the hydroxyapatite samples. The effect of fluoride ion addition may clearly be seen when examining the Ca(2)–OH bond length. The values of the Ca(2)–OH bond length were significantly higher for HA05F and HA025F than for HA. This may be attributed to the fact that the fluoride ions substituted for OH groups in the apatite lattice and since the fluoride group has a larger ionic radius than that of the OH group, more

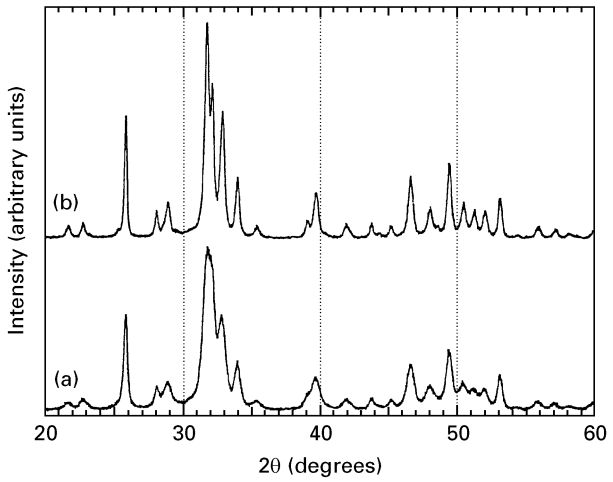

Figure 4 X-ray diffraction spectra for HA025F samples precipitated at (a) 3 °C and (b) 90 °C.

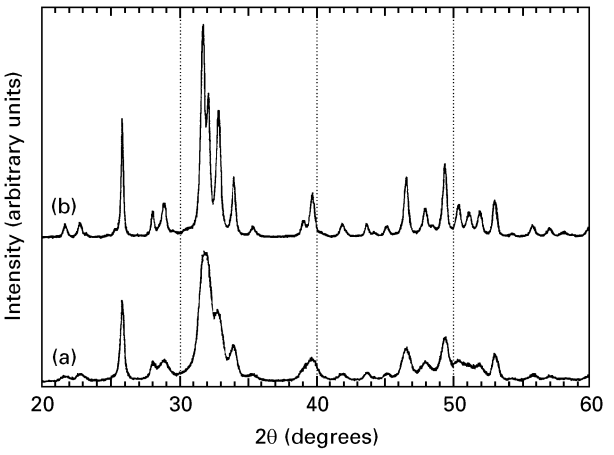

Figure 5 X-ray diffraction spectra for HA05F samples precipitated at (a) 3 °C and (b) 90 °C.

TABLE I Unit cell dimensions and unit cell volume of HA and fluoride-substituted apatites

Specimen	*a* axis (nm)		*c* axis (nm)		Volume (nm^3)	
	3 °C	90 °C	3 °C	90 °C	3 °C	90 °C
HA	0.9432	0.9431	0.6882	0.6898	0.5301	0.5308
HA025F	0.9421	0.9419	0.6880	0.6886	0.5287	0.5289
HA05F	0.9417	0.9419	0.6880	0.6888	0.5282	0.5291

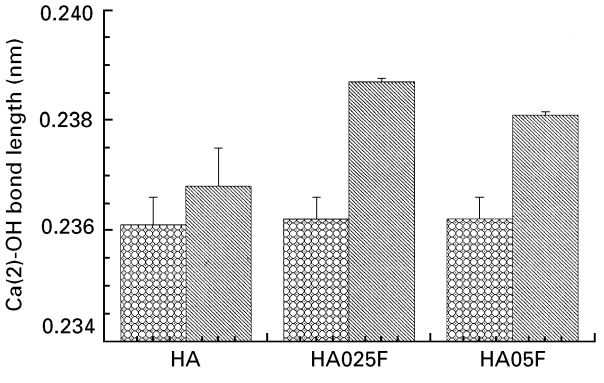

Figure 6 Ca (2)-OH bond length of hydroxyapatite and fluoride-substituted apatites precipitated at ▨ 3 °C, and ▨ 90 °C.

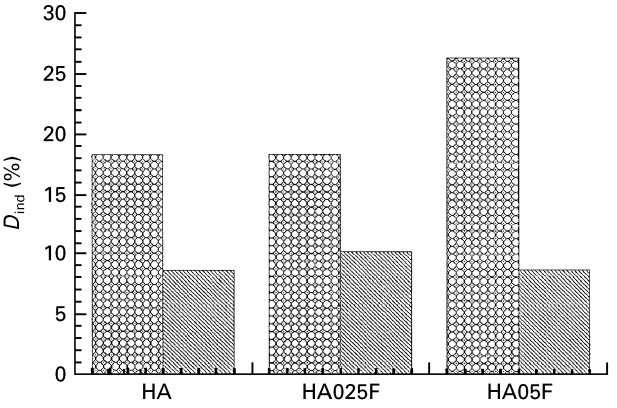

Figure 7 Distortion index of hydroxyapatite and fluoride-substituted apatites precipitated at ▨ 3 °C, and ▨ 90 °C.

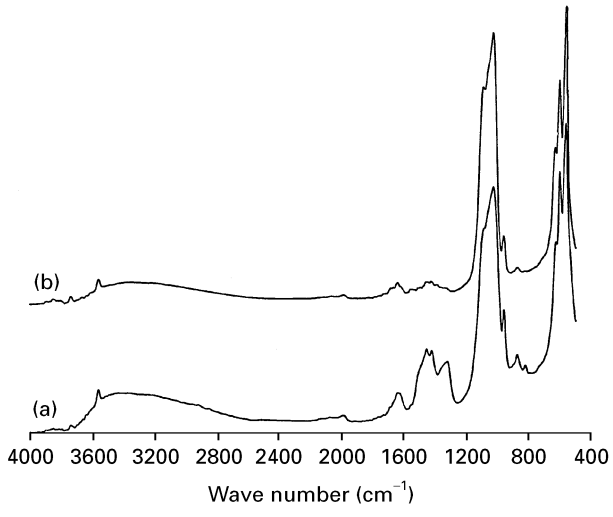

Figure 8 FTIR spectra of apatites precipitated at 3 °C: (a) HA; and (b) HA025F.

distortion was observed in the fluoride-substituted apatites than in HA.

5. Conclusion

Hydroxyapatite and fluoride-substituted apatite crystallites were small and spheroidal in morphology at precipitation temperatures of 3 and 25 °C, and became increasingly large and more acicular at higher precipitation temperatures. The addition of fluoride ions for any given reaction temperature appeared to reduce the aspect ratio of the crystallites. X-ray diffraction analysis and transmission electron microscopy indicated that the crystallinity of the 3 °C samples was lower than that of the 90 °C samples. A significant increase in the Ca(2)–OH bond length of fluoride-substituted

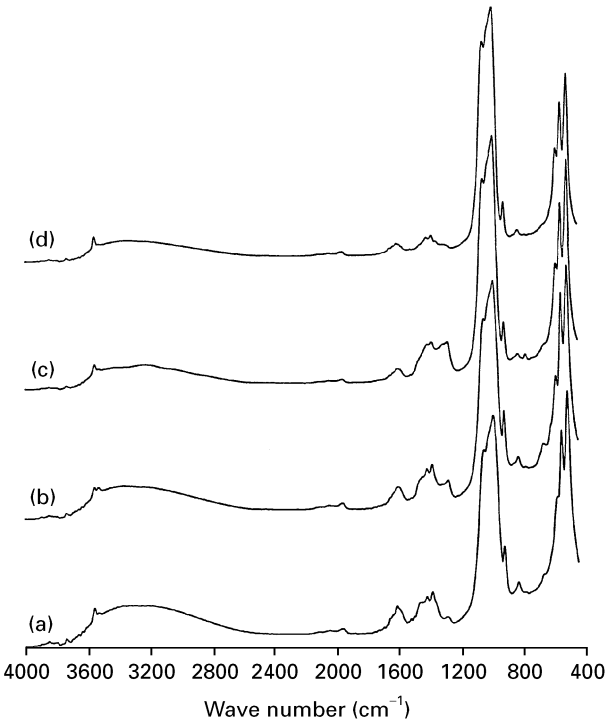

Figure 9 FTIR spectra of HA05F precipitated at (a) 3°, (b) 25°, (c) 60° and (d) 90°C.

apatites was observed due to the incorporation of fluoride ions in the lattice, and also a marked decrease in *a* axis dimension was observed in the fluoride-substituted apatites with increasing fluoride ion substitution.

Acknowledgements

One of the authors (LJJ) would like to thank JNICT, Portugal, for the financial support under PRAXIS XXI/BPD/4122/94 programme to carry out this work. JDs would like to thank PBIC/C/CTM/1890/95 JNICT, Portugal for support in this project. The authors would like to thank Professor J. Elliot, Child Dental Care Department, London Hospital, London, for helpful discussions and Mr M. Willis, QMW College, for assistance with transmission electron microscopy. The support of EPSRC for the core programme of the IRC in Biomedical Materials is gratefully acknowledged.

References

1. F. BETTS, C. NORMAN and S. R. POSNER, *J. Cryst. Growth* **53** (1981) 63.
2. I. ARENDS I and I. M. TENCATE, *ibdi.* **53** (1981) 135.
3. G. BOIVIN and P. J. MEUNIER, in "The metabollic and molecular basis of acquired disease", edited by R. D. Cohen, B. Lewis, K. G. M. M. Alberti and A. M. Desman (Bailliere Tindall, London, 1990).
4. W. G. M. VAN DEN HOCK, T. P. FENSTRA and P. L. deBRUYN, *J. Phys. Chem.* **84** (1980) 3312.
5. R. Z. LeGEROS, R. KIJKOWSKA, W. JIA and J. P. LeGEROS, *J. Fluorine Chem.* **41** (1988) 53–64.
6. J. P. BARONE and G. H. NANCOLLAS, *J. Dent. Res.* **57** (1978) 735–742.
7. E. C. MORENO, M. KREWASK, R. T. ZAHRADINK, *Nature* **247** (1974) 64.
8. G. H. NANCOLLAS, Z. AHMED and P. KOUTSOUKOS, in "ACS Symposium Series", Vol. 93, pp. 475–497 (American Chemical Society, Washington, DC, 1979).
9. E. C. MORENO and K. VARUGHESE, *J. Cryst. Growth* **53** (1981) 20.
10. P. PANTUMVANIT, F. F. FEAGIN and T. KOULOURIDES, *Caries Res.* **11** (1977) 52.
11. I. L. MEYER and G. H. NANCOLLAS, *J. Dent. Res.* **51** (1972) 1443.
12. K. ISHIKAWA, E. D. EANES and M. S. TUNG, *ibid.* **73** (1994) 1462.
13. E. DUFF, *J. Chem. Soc.* A, (1971) 33.
14. F. C. M. DRIESSENS, in "Bioceramics of calcium phosphate", edited by K. deGroot (CRC Press, Boca Raton, FL, 1988), pp. 1–33.
15. J. CHRISTOFFERSEN, M. R. CHRISTOFFERSEN and T. JOHANSEN, in 12th European Conference of Biomaterials, Porto, Portugal, 1995.
16. J. CHRISTOFFERSEN, *J. Cryst. Growth* **49** (1980) 29.
17. M. R. CHRISTOFFERSEN, J. CHRISTOFFERSEN and W. KIBALCZYC, *ibid.* **106** (1990) 349.
18. M. R. CHRISTOFFERSEN and J. CHRISTOFFERSEN, *ibid.* **121** (1990) 349.
19. K. S. TENHUISEN and P. W. BROWN, *J. Dent. Res.* **73** (1994) 598.
20. K. KANDORI, A. YASUKAWA and T. ISHIKAWA, *Chem. Mater.* **7** (1995) 26.
21. K. ISHIKAWA, E. D. EANES and M. S. TUNG, *J. Dent. Res.* **73** (1994) 1462.
22. S. V. DOROZHKIN, *Russian J. Inorg. Chem.* **39** (1994) 217.
23. A. C. LARSON, R. B. Von DREELE and M. LUJAN Jr., "GSAS-Generalised Crystal Structure Analysis System". Neutron Scattering Centre, Los Alamos National Laboratory, California (1990).
24. I. ABRAHAMS and J. C. KNOWLES, *J. Mater. Chem.* **4** (1994) 185.

Received 7 May
and accepted 11 July 1996